A 80-kW Isolated DC–DC Converter for Railway Applications

Nico H. Baars, *Student Member, IEEE*, Jordi Everts, *Member, IEEE*, Henk Huisman, Jorge L. Duarte, *Member, IEEE*, and Elena A. Lomonova, *Senior Member, IEEE*

***Abstract*—This paper provides an analysis of a three-phase dual active bridge (DAB) topology used as high-power-density dc–dc converter for railway applications. The three-phase DAB is analyzed concerning the current intervals, the output power, and soft-switching region, including the impact of zero-voltage switching capacitors. Furthermore, two measures are proposed to achieve soft-switching in the entire operating range, being auxiliary inductors and a straightforward switching strategy called the burst mode. Optimal component values are calculated to minimize losses in the complete operating range and to assess which measure is best suited. A prototype with the specifications acquired from the application has been built, yielding an efficiency of 95.6% at a nominal output power of 80 kW.**

***Index Terms*—DC–DC power conversion, power electronics, power supplies, rail transportation electronics.**

I. Introduction

SINCE the electrification of rail transportation systems, the amount of additional electrical systems in the vehicle has been increasing substantially. These, so called "auxiliary systems" are all systems on a rail vehicle that have functions other than traction. Nowadays, many auxiliary systems are present on rail vehicles. Examples are lighting, compressors, pumps, air-conditioning, and passenger information systems. In order to provide energy to these auxiliary systems, an auxiliary power unit (APU) converts the voltage from the overhead line or a third rail to the required levels of supply voltages. The total auxiliary power demand is typically in the range of tens of kilowatts up to a few hundreds of kilowatts. For safety reasons, galvanic isolation between the input and the output of the APU is required. In conventional APUs, the galvanic isolation is often realized with low-frequency transformers, an example is shown in Fig. 1(a). These transformers are bulky and result in relatively large and heavy APUs. Especially for light rail vehicles, like trams and metros, this becomes a problem when the auxiliary power demand increases. Therefore, size and weight reduction of the APU is necessary to meet the auxiliary power demand within the capabilities of light rail vehicles.

Most of the light rail transport systems are using a dc electrification system with common nominal voltages of 600 or 750 V.

Manuscript received October 1, 2014; revised December 11, 2014; accepted January 6, 2015. Date of publication January 23, 2015; date of current version August 21, 2015. Recommended for publication by Associate Editor D. Vinnikov.

The authors are with the Department of Electrical Engineering, Eindhoven University of Technology, Eindhoven 5600MB, The Netherlands (e-mail: n.h.baars@tue.nl; j.everts@tue.nl; h.huisman@tue.nl; j.l.duarte@tue.nl; e.lomonova@tue.nl).

Color versions of one or more of the figures in this paper are available online at http://ieeexplore.ieee.org.

Digital Object Identifier 10.1109/TPEL.2015.2396006

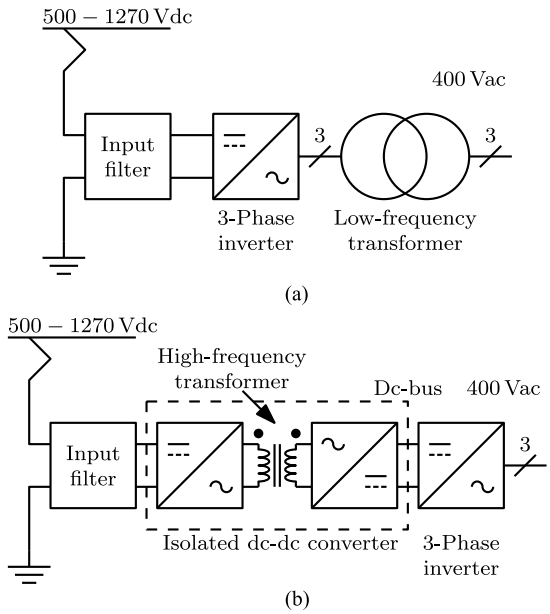

Fig. 1. Simplified schematic of an APU. (a) Conventional APU. (b) Proposed APU.

TABLE I
Requirements for the Investigated DC–DC Converter

Requirement	Value
Input voltage range	500–900 V
Peak input voltage	1270 V
Output voltage	600V
Continuous output power	80 kW
Switching frequency	20 kHz

Adding an isolated dc–dc converter is the preferable solution for reducing size and weight of the APU. By placing the isolated dc–dc converter between the input filter and the three-phase inverter, the bulky low-frequency transformer can be omitted, as can be seen in Fig. 1(b). This paper focuses on the design of an isolated dc–dc converter for railway applications. The requirements for the investigated dc–dc converter are presented in Table I.

In Section II, the results of several publications concerning power density, soft-switching techniques, and comparison of different topologies are discussed.

II. Topology Overview

The field of high-power-density dc–dc converters has been addressed often in the last decades. From the beginning,

the conventional full-bridge converter topology has been the preferred choice to realize a high-power dc–dc converter [1]. However, due to problems with the leakage inductance of the transformer and, consequently, reverse recovery losses of the output diodes, the maximum switching frequency is limited. To solve this problem, several solutions were presented, including active clamps and/or auxiliary circuits [2]–[4]. These solutions enable higher switching frequencies at the expense of additional components and could lead to higher device stress. The additional components impede the increase in power density and increased complexity, while the efficiency is often not better compared to other zero-voltage switching (ZVS) and zero-current switching (ZCS) techniques.

Resonant converter topologies offer possibilities for ZVS or ZCS, enabling high efficiencies and power densities [5]–[7]. The series resonant or LLC converter provides a load independent operating point with unity voltage gain at a switching frequency near the resonance frequency [6], [8]–[10]. However, this load independent operating point is lost when the input and/or output voltage changes, and switching frequency control is necessary to regulate the output voltage. Therefore, a boost converter can be used to regulate the input voltage in order to guarantee operation in the load independent operating point [10], [11]. Alternatively, the resonance circuit can be influenced by a switch-controlled capacitor, resulting in fixed frequency operation [12]. Despite the provided solutions, the LLC converter still suffers from high rms phase currents, requiring a relatively large series resonant capacitor that leads to a decreased power density. The additional boost converter or switch-controlled capacitor also deteriorates the power density and efficiency.

The dual active bridge (DAB) topology introduced in [1] is an attractive alternative to the problems with the classical full-bridge topology. In comparison with the conventional full-bridge topology, the output inductor is transferred to the ac side, and is in series with the leakage inductance. Consequently, the energy in the leakage inductance is transferred to the load without causing reverse recovery losses in the output diodes. This allows higher switching frequencies and, therefore, an increase in power density. Furthermore, the use of an active output bridge also increases the power density of the transformer [1]. When the desired inductance can be incorporated in the transformer, again the power density can be increased. In [13], very high power densities, up to $11.13\,\mathrm{kW/L}$, are reported.

A three-phase DAB, also proposed in [1], has some advantages in comparison to the single-phase DAB. The three-phase DAB has lower turn-off currents in the switches and lower rms currents per phase. Also, the VA ratings for the input and output filters are significantly lower and can even go to zero due to the three-phase characteristics. Besides the lower VA ratings, the effective ripple frequency of the filter currents is three times higher, allowing to use smaller filters. Compared to the single-phase DAB, the currents through the transformer windings are much more sinusoidal, resulting in reduced high-frequency losses in the transformers [14]. A comprehensive comparison of single-phase and three-phase DAB topologies is given in [1] and [15].

Both the single-phase and three-phase DAB topologies suffer from a limited soft-switching range in case the input voltage and the reflected output voltage are not equal. For the single-phase DAB, there exist switching strategies or modulation schemes for increasing the soft-switching range. These are described in [16]–[20]. Here, the soft-switching operating range is increased and also the overall efficiency can be increased with a minimum loss modulation strategy [21], [22]. The three-phase DAB does not possess these advantageous switching possibilities. The phase shift angle ϕ between the bridge voltage is the only control variable as the symmetrical properties of the three-phase system have to be maintained [14], [21].

Although the three-phase DAB has less switching possibilities, compared to the single-phase DAB, and includes four extra switches, the topology has the most preferred properties for designing a high-power density isolated dc–dc converter. It has the lowest component ratings and is capable of achieving higher output powers with possibly the highest power density. For APU applications in light rail vehicles, high-power capability and power density are decisive. Therefore, the three-phase DAB topology is selected in this study.

III. Three-Phase DAB DC–DC Converter

The three-phase DAB, shown in Fig. 2(a), consists of two three-phase bridges coupled with a three-phase transformer connected in Y–Y. The bridges are operated in six-step mode at a constant frequency. By applying a phase shift between the input and output bridge, the power flow can be controlled. Because the converter is symmetrical from input to output, bidirectional power flow is possible. The transformer leakage inductances are used as current transfer elements and, therefore, not considered as parasitic. If the magnetizing inductance L_m is neglected, an equivalent circuit can be used for analysis. In this circuit, only the total leakage inductance L_s seen from the primary side is connected between the phase legs from the input and output bridge. The corresponding idealized waveforms are shown in Fig. 2(b).

A. Analysis

To analyze the soft-switching region, the current of phase A is defined for the first six intervals as depicted in Fig. 2(b). The current i_A in the different intervals is given in (3) for phase shifts of $0 \leq \phi \leq \frac{\pi}{3}$. For phase shifts of $\frac{\pi}{3} \leq \phi \leq \frac{2\pi}{3}$, a second set of equations, not given here, is utilized for further analysis of the soft-switching region. The magnetizing inductance L_m of the transformer is neglected in the analysis.

Furthermore, the angular frequency is defined as $\omega = 2\pi f_\mathrm{s}$, with f_s the switching frequency in Hertz. The transformer's leakage inductance is indicated with L_s and the input and output voltage are defined as V_i and V_o, respectively. The reflected output voltage is given by $V_\mathrm{o}' = V_\mathrm{o} N$, with N the turns ratio of the transformer.

Because the phase current is symmetric, the current $i_\mathrm{A}(0)$ can be found by solving the set of equations, assuming steady-state

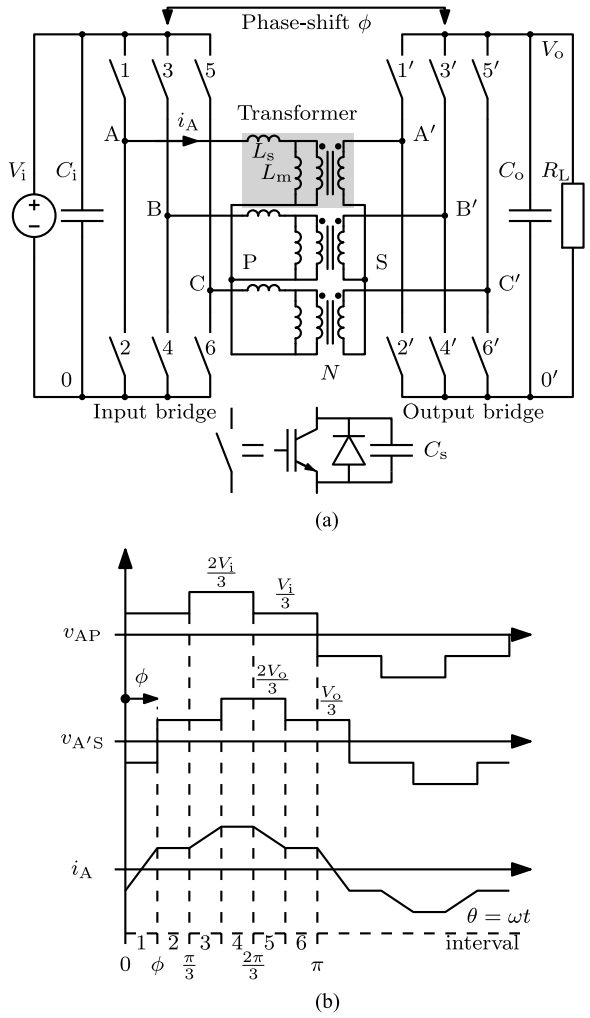

Fig. 2. Three-phase DAB. (a) Topology. (b) Idealized waveforms, gating signals can be found in [1].

condition $i_\mathrm{A}(0) = -i_\mathrm{A}(\pi)$. This results in

$$i_\mathrm{A}(0) = \frac{1}{3\omega L_\mathrm{s}}\left[\frac{2\pi}{3}(V_\mathrm{o}' - V_\mathrm{i}) - V_\mathrm{o}'\phi\right]. \tag{1}$$

B. Output Power

Under the assumption of a lossless converter, the output power P_o can be found with

$$P_\mathrm{o} = P_\mathrm{i} = \frac{3}{\pi}\int_0^\pi v_\mathrm{AP}(\theta) i_\mathrm{A}(\theta) d\theta. \tag{2}$$

Finally, the expression of the output power for $0 \le \phi \le \frac{2\pi}{3}$ is

$$P_\mathrm{o} = \begin{cases} \frac{V_\mathrm{i}V_\mathrm{o}'}{\omega L_\mathrm{s}}\phi\left[\frac{2}{3} - \frac{\phi}{2\pi}\right] & \text{for } 0 \le \phi \le \frac{\pi}{3} \\ \frac{V_\mathrm{i}V_\mathrm{o}'}{\omega L_\mathrm{s}}\left[\phi - \frac{\phi^2}{\pi} - \frac{\pi}{18}\right] & \text{for } \frac{\pi}{3} \le \phi \le \frac{2\pi}{3}. \end{cases} \tag{4}$$

C. Soft-Switching Region

Minimizing the switching losses is the key to achieve a high switching frequency. The turn-on losses are of main interest because excessive losses in the switch and the antiparallel diode can arise when the antiparallel diodes experience the reverse recovery process. The input bridge faces this problem when $i_\mathrm{A}(0) > 0$. Therefore, the current has to fulfill $i_\mathrm{A}(0) \le 0$ to ensure soft-switching in the input bridge. During the switching transient, the current i_A is considered constant. Rewriting (1) to the required constraint gives the phase shift for ensuring soft turn-on of the switches in the input bridge, this is found to be

$$\phi_\mathrm{i} \ge \frac{2\pi(V_\mathrm{o}' - V_\mathrm{i})}{3V_\mathrm{o}'}. \tag{5}$$

A similar derivation can be made for the output bridge, where the output bridge is soft-switching for $i_A(\phi) \ge 0$. Using (3) and (1) gives the required phase shift to ensure soft turn-on of the switches in the output bridge, resulting in

$$\phi_\mathrm{o} \ge \frac{2\pi(V_\mathrm{i} - V_\mathrm{o}')}{3V_\mathrm{i}}. \tag{6}$$

1) Impact of ZVS Capacitors: ZVS capacitors, or snubber capacitors, are used to reduce turn-off losses. These are connected in parallel to the switches and supplement the output capacitance, as can be seen in Fig. 2(a). After a switch turns OFF, there is a small blanking time t_b before the opposite switch of the same leg turns on. During t_b, the current commutates to the ZVS capacitors and divides equally over the two capacitors of the phase leg. In this transition, one capacitor is charged while the other is discharged. This implies that the load current must be high enough to enable a full charge or discharge of the ZVS capacitors for a given t_b. Assuming a constant current during the switching transient, the soft-switching constraint for enabling soft turn-on of the switches in the input bridge is changed to

$$i_\mathrm{A}(0) + \frac{2C_\mathrm{s}V_i}{t_\mathrm{b}} \le 0 \tag{7}$$

and for the output bridge to

$$i_\mathrm{A}(\phi) - \frac{2C_\mathrm{s}V_\mathrm{o}}{t_\mathrm{b}N} \ge 0 \tag{8}$$

$$i_\mathrm{A}(\theta) = \begin{cases} i_\mathrm{A}(0) + \frac{V_\mathrm{i}+V_\mathrm{o}'}{3\omega L_\mathrm{s}}\theta & \forall \quad 0 \le \theta \le \phi & \text{:interval 1} \\ i_\mathrm{A}(\phi) + \frac{V_\mathrm{i}-V_\mathrm{o}'}{3\omega L_\mathrm{s}}(\theta - \phi) & \forall \quad \phi \le \theta \le \frac{\pi}{3} & \text{:interval 2} \\ i_\mathrm{A}(\frac{\pi}{3}) + \frac{2V_\mathrm{i}-V_\mathrm{o}'}{3\omega L_\mathrm{s}}(\theta - \frac{\pi}{3}) & \forall \quad \frac{\pi}{3} \le \theta \le \frac{\pi}{3} + \phi & \text{:interval 3} \\ i_\mathrm{A}(\frac{\pi}{3} + \phi) + \frac{2V_\mathrm{i}-2V_\mathrm{o}'}{3\omega L_\mathrm{s}}(\theta - \frac{\pi}{3} - \phi) & \forall \quad \frac{\pi}{3} + \phi \le \theta \le \frac{2\pi}{3} & \text{:interval 4} \\ i_\mathrm{A}(\frac{2\pi}{3}) + \frac{V_\mathrm{i}-2V_\mathrm{o}'}{3\omega L_\mathrm{s}}(\theta - \frac{2\pi}{3}) & \forall \quad \frac{2\pi}{3} \le \theta \le \frac{2\pi}{3} + \phi & \text{:interval 5} \\ i_\mathrm{A}(\frac{2\pi}{3} + \phi) + \frac{V_\mathrm{i}-V_\mathrm{o}'}{3\omega L_\mathrm{s}}(\theta - \frac{2\pi}{3} - \phi) & \forall \quad \frac{2\pi}{3} + \phi \le \theta \le \pi & \text{:interval 6} \end{cases} \tag{3}$$

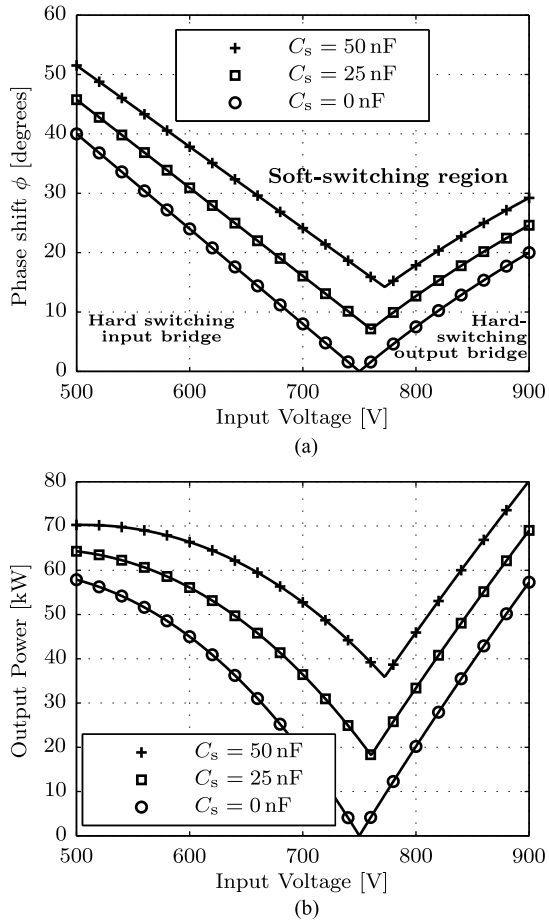

Fig. 3. Soft-switching region for $V_o' = 750$ V, $L_s = 20\,\mu$H, $f_s = 20$ kHz and $t_b = 5\,\mu$s. (a) Phase shift versus input voltage. (b) Output power versus input voltage.

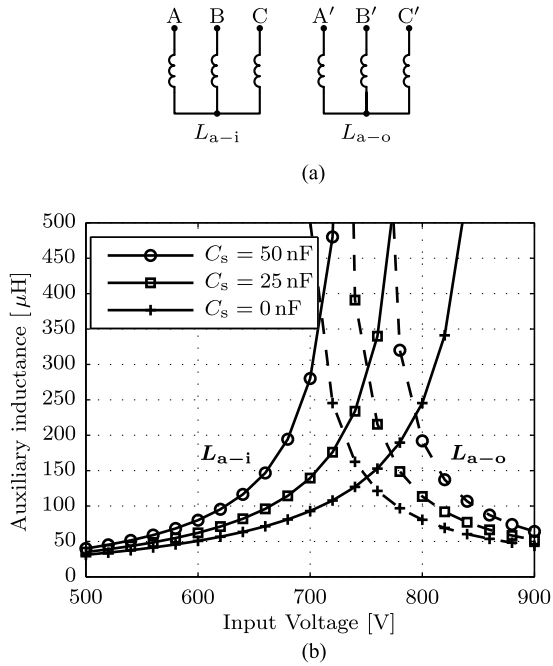

Fig. 4. Auxiliary inductors, $V_o' = 750$V, $L_s = 20\,\mu$H, $f_s = 20\,$kHz and $t_b = 5\,\mu$s. (a) Connection of the auxiliary inductors. (b) Required inductance for the auxiliary inductors.

where C_s represents a ZVS capacitor connected in parallel to the switch, and t_b is a fixed blanking time. A more accurate, current depending charge-based ZVS analysis is reported in [20]. However, to investigate the impact of the ZVS capacitors and approximate the soft-switching region, the presented current-based method is sufficient.

Solving (7) and (8) for the phase-shift ϕ gives the soft-switching region for the input bridge and the output bridge, respectively. These are given by

$$\phi_i \geq \frac{2\pi_i(V_o' - V_i)}{3V_o'} + \frac{2C_s V_i}{V_o' t_b} 3\omega L_s \tag{9}$$

and

$$\phi_o \geq \frac{2\pi(V_i - V_o')}{3V_i} + \frac{2C_s V_o}{V_i t_b N} 3\omega L_s. \tag{10}$$

When satisfying both (9) and (10), a soft-switching region can be defined as function of the input voltage V_i, as shown in Fig. 3(a). The input voltage varies from 500 to 900 V, which is given in Table I for light rail vehicles with a nominal voltage of 750 V. The reflected output voltage V_o' is chosen to equal the nominal input voltage of 750 V to have a good utilization of the soft-switching region. Furthermore, the blanking time is chosen to be 10% of the switching cycle that means a duration of 5 μs.

The soft-switching region can also be presented as the minimum output power versus the input voltage. An example is presented in Fig. 3(b) with the leakage inductance L_s set to 20 μH.

Fig. 3(a) and (b) shows that the ZVS capacitors decrease the soft-switching region. Especially, Fig. 3(b) shows the limitations for low- and high-input voltages. Therefore, the next section describes two methods to extend the soft-switching region.

D. Extension of the Soft-Switching Region

Auxiliary power converters for railway applications have to be able to operate from no-load to full-load conditions over the whole input voltage range. This means that the converter has to operate outside the soft-switching region. Therefore, two methods to extend the soft-switching operation of the converter have been investigated.

1) Auxiliary Inductors: The first method is based on adding reactive currents to fully charge or discharge the ZVS capacitors during the switching transient. The reactive currents are injected with three star-connected auxiliary inductors per bridge, as can be seen in Fig. 4(a). This has the same effect as the magnetizing inductances of the transformers, which are also connected in star [23]. However, separate auxiliary inductors are preferred to have more design flexibility.

The peak current, injected by the auxiliary inductors during the switching transient, is calculated from the voltage waveforms shown in Fig. 2(b). For the input bridge, the peak current is calculated as

$$\hat{i}_{a-i} = \frac{2\pi V_i}{9\omega L_{a-i}} \tag{11}$$

and for the output bridge as

$$\hat{i}_{\mathrm{a-o}} = \frac{2\pi V_{\mathrm{o}}}{9\omega L_{\mathrm{a-o}} N}. \tag{12}$$

Next, the soft-switching constraints from (7) and (8) can be extended to

$$i_{\mathrm{A}}(0) + \frac{2C_{\mathrm{s}}V_{\mathrm{i}}}{t_{\mathrm{b}}} - \frac{2\pi V_{\mathrm{i}}}{9\omega L_{\mathrm{a-i}}} \leq 0 \tag{13}$$

and for the output bridge to

$$i_{\mathrm{A}}(\phi) - \frac{2C_{\mathrm{s}}V_{\mathrm{o}}}{t_{\mathrm{b}}N} + \frac{2\pi V_{\mathrm{o}}}{9\omega L_{\mathrm{a-o}}N} \geq 0. \tag{14}$$

Then, the soft-switching region can be calculated with the minimum phase shift for the input bridge

$$\phi_{\mathrm{i}} \geq \frac{2\pi(V_{\mathrm{o}}' - V_{\mathrm{i}})}{3V_{\mathrm{o}}'} + \frac{2C_{\mathrm{s}}V_{\mathrm{i}}}{V_{\mathrm{o}}'t_{\mathrm{b}}}3\omega L_{\mathrm{s}} - \frac{2\pi V_{\mathrm{i}}L_{\mathrm{s}}}{3V_{\mathrm{o}}'L_{\mathrm{a-i}}} \tag{15}$$

and for the output bridge

$$\phi_{\mathrm{o}} \geq \frac{2\pi(V_{\mathrm{i}} - V_{\mathrm{o}}')}{3V_{\mathrm{i}}} + \frac{2C_{\mathrm{s}}V_{\mathrm{o}}}{V_{\mathrm{i}}t_{\mathrm{b}}N}3\omega L_{\mathrm{s}} - \frac{2\pi V_{\mathrm{o}}L_{\mathrm{s}}}{3V_{\mathrm{i}}L_{\mathrm{a-o}}N}. \tag{16}$$

As shown with (15) and (16), the auxiliary inductance decreases the required phase-shift for operating in a soft-switching manner. To achieve soft-switching in the whole operating range, (15) and (16) should be solved for zero phase-shift, i.e., no-load condition. The corresponding values are shown in Fig. 4(b). For relatively low- and high-input voltages, the required values for $L_{\mathrm{a-i}}$ and $L_{\mathrm{a-o}}$ are low and, therefore, also causing high reactive currents. The use of auxiliary inductors presents a clear disadvantage due to the reduced efficiency and power density.

2) Burst Mode: The second method does not use any extra components but relies on a straightforward switching strategy. When the required output power P_{o} is lower than the minimum load for soft switching, the converter switches from continuous mode to burst mode. In the burst mode, the converter operates with an output power P_{b} high enough to enable soft-switching. An example of the burst mode with the corresponding waveforms is shown in Fig. 5(a). The average output power is defined as

$$< p_{\mathrm{o}} >= \frac{n}{m}P_{\mathrm{b}}, \qquad \forall \quad 1 \leq n \leq m \tag{17}$$

where n is the amount of switching cycles operating with $p_{\mathrm{o}} = P_{\mathrm{b}}$ and m is the total amount of switching cycles of one burst cycle. The value of P_{b} depends on the soft-switching region of the converter, an example is given in Fig. 3(b).

When $nT_{\mathrm{s}} < t \leq mT_{\mathrm{s}}$, the output power $p_{\mathrm{o}} = 0$ W, thus the output capacitor delivers the required current to the load, introducing a small voltage ripple. The output voltage ripple can be calculated with

$$\Delta v_{\mathrm{o}} = \frac{I_{\mathrm{o}}\Delta t}{C_{\mathrm{o}}} \tag{18}$$

where $I_{\mathrm{o}} = \frac{<p_{\mathrm{o}}>}{V_{\mathrm{o}}} = \frac{nP_{\mathrm{b}}}{mV_o}$ and $\Delta t = \frac{m-n}{f_{\mathrm{s}}}$. This results in

$$\Delta v_{\mathrm{o}} = \frac{n(m-n)P_{\mathrm{b}}}{mV_{\mathrm{o}}C_{\mathrm{o}}f_{\mathrm{s}}}. \tag{19}$$

An example of the output voltage ripple with $n \geq 2$ is shown in Fig. 5(b).

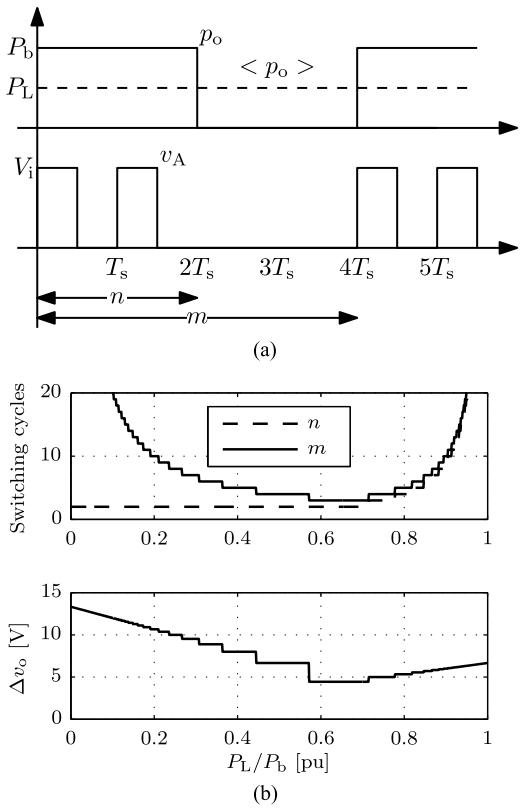

Fig. 5. Burst-mode waveforms. (a) Burst-mode definitions. (b) Output voltage ripple with $n \geq 2$, $P_{\mathrm{b}} = 80\,\mathrm{kW}$, $V_{\mathrm{o}} = 600\,\mathrm{V}$, $C_{\mathrm{o}} = 1\,\mathrm{mF}$, and $f_{\mathrm{s}} = 20\,\mathrm{kHz}$.

The downside of this method is the need for a larger output capacitance for the same voltage ripple requirements in normal operation without the burst mode. Furthermore, while the switching frequency is unchanged, the converter becomes audible due to the discontinuous operation.

IV. Prototype Design

A prototype was designed and built according to the specifications from Table I. The transformer winding-ratio *N* is chosen to equal $750:600$ or correspondingly $5:4$. In this case, the reflected output voltage is equal to the nominal input voltage, resulting in a good soft-switching region at the nominal input voltage. The switches in the input and output bridge are implemented with three-phase IGBT modules from Semikron type SKiM429GD17E4HD.

Optimal values have been calculated for the leakage inductance L_{s}, ZVS capacitors C_{s} and the auxiliary inductor L_{a}. The goal is to minimize the overall losses by varying L_{s} and C_{s}. While L_{a}, if necessary, is used to maintain soft-switching at maximum power. In this way, the burst mode can be employed for output powers below the maximum output power.

The losses are calculated at maximum output power over the entire feasible component value range while operating at $V_{\mathrm{i}} = 500$, 750, and 900 V, covering the full input voltage range. The calculated losses are given by

$$P_{\mathrm{loss}} = (E_{\mathrm{off}})f_{\mathrm{s}} + P_{\mathrm{cond}} + P_{\mathrm{cu}} + P_{\mathrm{core}} + P_{\mathrm{aux}} \tag{20}$$

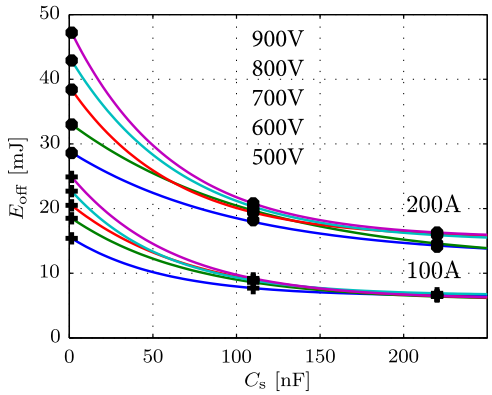

Fig. 6. Turn-off losses, for SKiM429GD17E4HD, are curve fitted with measured points. For $V_{\rm i} = 500 - 900\,{\rm V}$ with turn-off currents $I_{\rm c} = 100\,{\rm A}$ and $I_{\rm c} = 200\,{\rm A}$ versus $C_{\rm s}$.

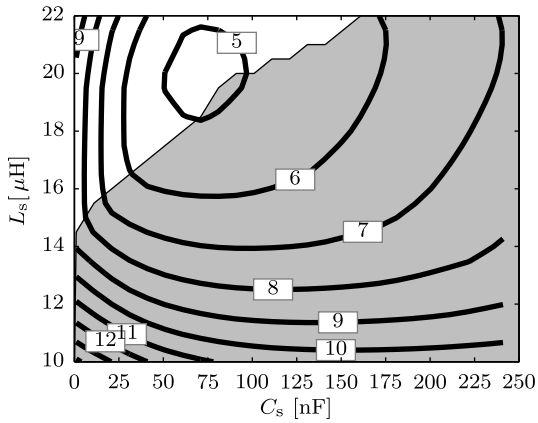

Fig. 7. Average losses (5–12 kW) of the converter operating at $P_{\rm o} = 80\,{\rm kW}$ for $V_{\rm i} = 500, 750$, and $900{\rm V}$.

with $E_{\rm off} = E_{\rm off-input} + E_{\rm off-output}$ representing both the turn-off losses of the input and output bridge, $P_{\rm cond}$ is the total IGBT and diode conduction losses of the input and output bridge, $P_{\rm cu}$ is the total ohmic loss of the transformer windings including the leakage inductance $L_{\rm s}$, The total core loss is indicated by $P_{\rm core}$ and $P_{\rm aux}$ is the power consumption of the control, driver, and measurement boards.

A series of measurements was performed to obtain the IGBT turn-off losses with different ZVS capacitors, turn-off voltages, and turn-off currents. Waveforms of the switch voltage and current are presented in the experimental results section. The measured turn-off losses are interpolated with an exponential curve for each turn-off voltage. The current dependency is approximated by a linearizion at the reference turn-off current $I_{\rm c}^*$. The turn-off losses are given by

$$E_{\rm off} = (x_1 \cdot e^{-x_2 \cdot C_{\rm s}} + x_3)\frac{I_{\rm c}}{I_{\rm c}^*} \tag{21}$$

with x_{1-3} the curve fitting parameters. The fitted curves and the measured data are shown in Fig. 6.

The result of the optimization is shown in Fig. 7, the contour plot shows the average losses of the converter operating at three given input voltages, the shaded area indicates the use

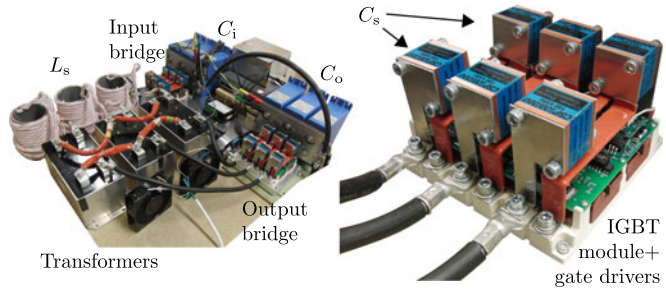

Fig. 8. 80-kW prototype, (left) complete setup and (right) three-phase IGBT module with ZVS capacitors $C_{\rm s}$ and gate drivers.

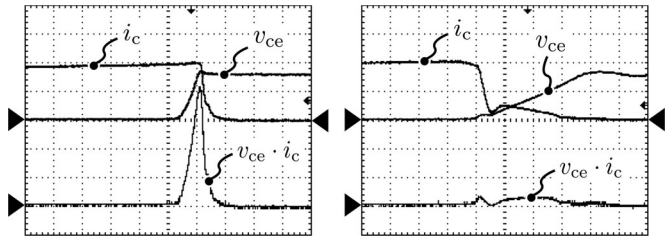

Fig. 9. Turn-off switching transients, with $I_{\rm c} = 100\,{\rm A}$, $V_{\rm ce} = 800\,{\rm V}$, (left) $C_{\rm s} = 0\,{\rm nF}$ and (right) $C_{\rm s} = 110\,{\rm nF}$. (200 V/div, 50 A/div, 20 kVA/div).

of the auxiliary inductors, $L_{\rm a}$. The minimum losses were found for $C_{\rm s} = 70\,{\rm nF}$, $L_{\rm s} = 20\,\mu{\rm H}$ and no auxiliary inductors were required. It is important to notice that this minimum is mainly depending on the turn-off switching energy of the chosen IGBT technology under ZVS operation, which was found empirically.

The prototype is built with the presented optimal values. The required leakage inductance of the transformer is realized by connecting a custom-made inductor in series with the primary winding of the transformer, as can be seen in Fig. 8. The ZVS capacitor had to be chosen from commercially available capacitors. The nearest available value, with the appropriate specifications, was $50\,{\rm nF}$. The IGBT module together with the ZVS capacitors are shown in Fig. 8.

V. Experimental Results

The prototype shown in Fig. 8 is built according to the specifications and the optimal design given in this paper.

A. Switching Transients

The switch voltage and current, during the switching transient, were measured under hard and soft turn-off conditions, the waveforms are presented in Fig. 9. Hard turn-off, with a turn-off current of $100\,{\rm A}$ and a turn-off voltage of $800\,{\rm V}$, is shown on the left side. Soft turn-off, under the same conditions with a ZVS capacitor of $110\,{\rm nF}$, is shown on the right side. As can be seen, the soft turn-off has almost zero voltage while the current is falling. However, the current tail, inherent with IGBTs, is still creating power loss. Nevertheless, in this experiment, the turn-off losses with a ZVS capacitor of $110\,{\rm nF}$ are measured to be only 40% of the hard switching losses.

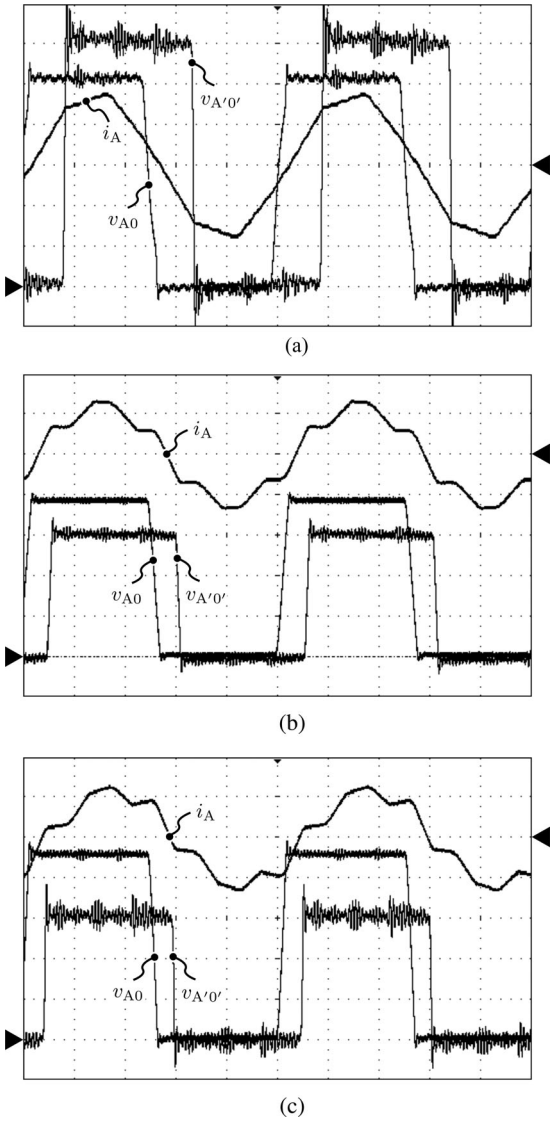

Fig. 10. Measured converter waveforms. (a) $V_i = 500\,V$ (100 V/div, 100 A/div, 10 μs/div), (b) $V_i = 750\,V$ (200 V/div, 100 A/div, 10 μs/div), and (c) $V_i = 900\,V$ (200 V/div, 100 A/div, 10 μs/div).

B. Voltage and Current Waveforms

Converter waveforms were measured for different input voltages and with an output power of 80 kW, these are shown in Fig. 10(a), (b), and (c). The voltages v_{A0} and $v_{A'0'}$ are measured on the first phase leg from the input and output bridge, respectively. The current i_A is measured in the first phase on the primary side of the transformer.

C. Continuous Mode

The efficiency of the converter, operating continuously at a nominal input voltage of 750 V, is shown in Fig. 11(a). The calculated losses are classified and compared with the measured total losses as shown in Fig. 12. For higher output power levels, the calculated and measured efficiencies correspond well. The deviation at $P_o = 44\,kW$ is explained by the converter operating on the boundary of the soft-switching region, as shown in Fig. 3(b).

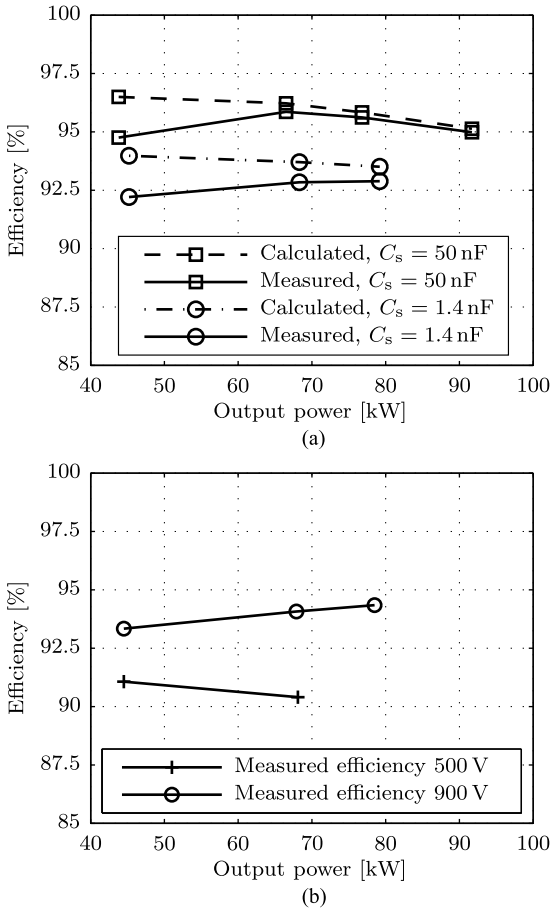

Fig. 11. Converter efficiency. (a) Efficiency in continuous mode with $V_i = 750\,V$. (b) Efficiency in burst mode with $V_i = 500\,V$ and $V_i = 900\,V$.

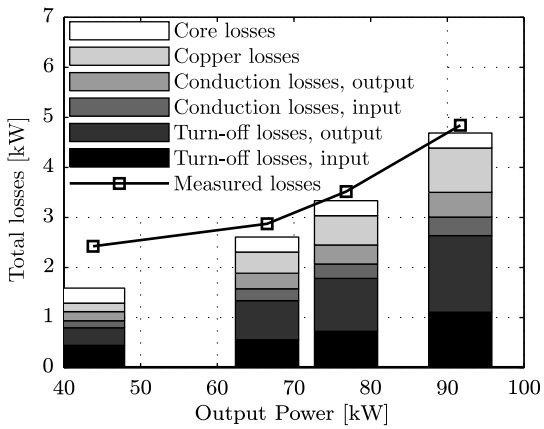

Fig. 12. Classification of the losses with $V_i = 750\,V$ and $C_s = 50\,nF$.

For comparison, the converter efficiency is also measured and calculated without the extra ZVS capacitors, as shown in Fig. 11(a). Without the ZVS capacitors, the converter efficiency is about 2% lower and was not able to operate above nominal output power because the high amount of losses.

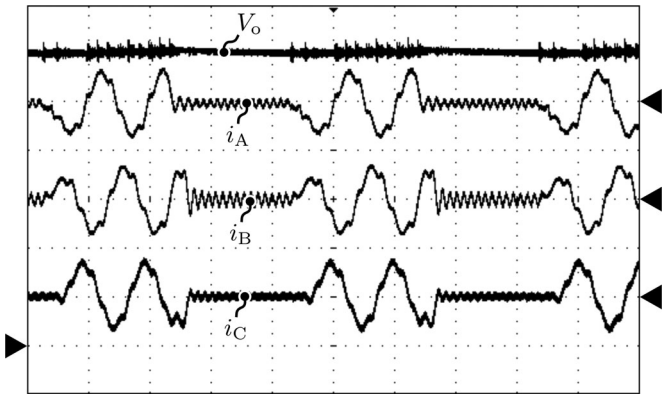

Fig. 13. Phase currents during burst mode with $m = 4$, $n = 2$, $V_i = 900\,\mathrm{V}$, $C_o = 1\,\mathrm{mF}$, $P_b = 80\,\mathrm{kW}$ and $P_o = 40\,\mathrm{kW}$ (200 A/div, 50 μs/div).

Furthermore, the soft-switching region, presented in Fig. 3(b), was verified by monitoring the IGBT module temperature in many different operating points. A significant increase of the IGBT module temperature can be seen when a transition from operating in the soft switching region to operation in the hard switching region occurs. The found boundary matches well with the calculated soft switching region.

D. Burst Mode

To supply the load from maximum to no-load conditions in the entire operating region, a burst mode is implemented, as described in the previous section. Fig. 13 shows the converter phase currents when operating in burst mode with an input voltage of $900\,\mathrm{V}$. The converter was supplying $40\,\mathrm{kW}$ of output power to the load. With $n = 2$ and $m = 4$, the converter processed only half of the burst power ($80\,\mathrm{kW}$). The switching frequency is still $20\,\mathrm{kHz}$, but due to the discontinuous operation, the converter is not inaudible anymore. The audible frequency for operation in the burst mode is f_s/m, which corresponds to $5\,\mathrm{kHz}$ for Fig. 13. A low amount of acoustic noise, produced in burst-mode operation, is audible when the converter is located in an open cabinet. A closed cabinet should be sufficient to reduce the acoustic noise to almost inaudible levels. Furthermore, the air coils in this experimental setup, representing the leakage inductance, are be responsible for a large part of the acoustic noise. Integrating the handmade coils in the transformer would solve this problem.

The efficiency during the burst mode, shown in Fig. 11(b), is lower compared to the continuous mode. The efficiency in burst-mode operation for an input voltage of 500 V drops by 1.5–2.5% with an output power range of 40–80 kW, respectively. For an input voltage of $900\,\mathrm{V}$, the efficiency drops in burst-mode operation by 1.5% . The reduced efficiency is caused by the first and last cycle in a complete burst cycle. The switches in the first cycle are not softly turned-on because the ZVS capacitors are not sufficiently charged, and the antiparallel diode is not conducting. This occurs due to a low switch turn-OFF current in the last cycle and the phase current being zero before the first cycle.

VI. Conclusion

The three-phase DAB topology has been selected for application in the APU because of the preferred properties concerning buck–boost operation, low device stress, small filters, high transformer utilization and low-switching losses. Subsequently, the soft-switching region is analyzed, including the effect of ZVS capacitors. Furthermore, two methods are presented to extend the soft-switching region: auxiliary inductors and a burst-mode switching strategy. Comprising a combination of the burst mode and auxiliary inductors, optimal component values are calculated to minimize the losses. As a result of the analysis, it is found that auxiliary inductors are not necessary with the use of the burst mode.

Experimental results show good agreement of measured waveforms with the idealized model. Furthermore, efficiencies of the burst and continuous mode with a measured efficiency of 95.6% at maximum output power at nominal conditions are presented. Also, the use of ZVS capacitors shows about 40% reduction of the total loss, enabling an output power above nominal and still preserving a good efficiency. The prototype was tested thoroughly in the entire operating range, including operation in the burst mode with an input voltage of 500 and $900\,\mathrm{V}$. The burst mode proves to be useful to extend the operating range in a soft-switching manner. Operation during burst mode shows slightly lower efficiencies compared to continuous operation.

Acknowledgment

The authors would like to thank Strukton Rolling Stock, in particular J. Verschoor and W. Platschorre, for their support.

References

[1] R. De Doncker, D. Divan, and M. Kheraluwala, "A three-phase soft-switched high-power-density dc/dc converter for high-power applications," *IEEE Trans. Ind. Appl.*, vol. 27, no. 1, pp. 63–73, Jan. 1991.

[2] J. Dudrik, P. Spanik, and N.-D. Trip, "Zero-voltage and zero-current switching full-bridge dc-dc converter with auxiliary transformer," *IEEE Trans. Power Electron.*, vol. 21, no. 5, pp. 1328–1335, Sep. 2006.

[3] J.-G. Cho, C.-Y. Jeong, and F. Lee, "Zero-voltage and zero-current-switching full-bridge PWM converter using secondary active clamp," *IEEE Trans. Power Electron.*, vol. 13, no. 4, pp. 601–607, Jul. 1998.

[4] O. Patterson and D. Divan, "Pseudo-resonant full bridge dc/dc converter," *IEEE Trans. Power Electron.*, vol. 6, no. 4, pp. 671–678, Oct. 1991.

[5] R. Steigerwald, "A comparison of half-bridge resonant converter topologies," *IEEE Trans. Power Electron.*, vol. 3, no. 2, pp. 174–182, Apr. 1988.

[6] A. Bhat and R. Zheng, "Analysis and design of a three-phase LCC-type resonant converter," *IEEE Trans. Aerospace and Electron. Syst.*, vol. 34, no. 2, pp. 508–519, Apr. 1998.

[7] R. Steigerwald, "High-frequency resonant transistor dc-dc converters," *IEEE Trans. Ind. Electron.*, vol. IE-31, no. 2, pp. 181–191, May 1984.

[8] X. Li, "A LLC-type dual-bridge resonant converter: Analysis, design, simulation, and experimental results," *IEEE Trans. Power Electron.*, vol. 29, no. 8, pp. 4313–4321, Aug. 2014.

[9] J.-W. Kim and G.-W. Moon, "A new LLC series resonant converter with a narrow switching frequency variation and reduced conduction losses," *IEEE Trans. Power Electron.*, vol. 29, no. 8, pp. 4278–4287, Aug. 2014.

[10] S. De Simone, C. Adragna, C. Spini, and G. Gattavari, "Design-oriented steady-state analysis of LLC resonant converters based on FHA," in *Proc. Int. Symp. Power Electron., Electr. Drives, Autom. Motion,*, May 2006, pp. 200–207.

[11] B.-C. Kim, K.-B. Park, C.-E. Kim, B.-H. Lee, and G.-W. Moon, "LLC resonant converter with adaptive link-voltage variation for a high-power-density adapter," *IEEE Trans. Power Electron.*, vol. 25, no. 9, pp. 2248–2252, Sep. 2010.

[12] Z. Hu, Y. Qiu, L. Wang, and Y.-F. Liu, "An interleaved LLC resonant converter operating at constant switching frequency," *IEEE Trans. Power Electron.*, vol. 29, no. 6, pp. 2931–2943, Jun. 2014.
[13] M. Pavlovsky, S. de Haan, and J. Ferreira, "Reaching high power density in multikilowatt dc-dc converters with galvanic isolation," *IEEE Trans. Power Electron.*, vol. 24, no. 3, pp. 603–612, Mar. 2009.
[14] H. Tao, J. Duarte, and M. Hendrix, "High-power three-port three-phase bidirectional dc-dc converter," in *Proc. 42nd IAS Annu. Meet. Conf. Rec. Ind. Appl. Conf.*, Sep. 2007, pp. 2022–2029.
[15] C. Dick, A. Konig, and R. De Doncker, "Comparison of three-phase dc-dc converters vs. single-phase dc-dc converters," in *Proc. 7th Int. Conf. Power Electron. Drive Syst.*, Nov. 2007, pp. 217–224.
[16] K. Vangen, T. Melaa, S. Bergsmark, and R. Nilsen, "Efficient high-frequency soft-switched power converter with signal processor control," in *Proc. 13th Int. Telecommun. Energy Conf.*, Nov. 1991, pp. 631–639.
[17] G. Oggier, R. Ledhold, G. Garcia, A. Oliva, J. Balda, and F. Barlow, "Extending the ZVS operating range of dual active bridge high-power dc-dc converters," in *Proc. 37th IEEE Power Electron. Spec. Conf.*, Jun. 2006, pp. 1–7.
[18] H. Tao, A. Kotsopoulos, J. Duarte, and M. Hendrix, "Transformer-coupled multiport ZVS bidirectional dc-dc converter with wide input range," *IEEE Trans. Power Electron.*, vol. 23, no. 2, pp. 771–781, Mar. 2008.
[19] J. Everts, F. Krismer, J. Van den Keybus, J. Driesen, and J. Kolar, "Optimal ZVS modulation of single-phase single-stage bidirectional dab ac-dc converters," *IEEE Trans. Power Electron.*, vol. 29, no. 8, pp. 3954–3970, Aug. 2014.
[20] J. Everts, F. Krismer, J. Van den Keybus, J. Driesen, and J. Kolar, "Charge-based ZVS soft switching analysis of a single-stage dual active bridge ac-dc converter," in *Proc. Energy Convers. Congr. Expo*, Sep. 2013, pp. 4820–4829.
[21] F. Krismer, "Modeling and optimization of bidirectional dual active bridge dc-dc converter topologies," Ph.D. dissertation, Power Electron. Systems Lab. ETH Zurich, Zurich, Switzerland, 2010.
[22] G. Oggier, G. Garcia, and A. Oliva, "Switching control strategy to minimize dual active bridge converter losses," *IEEE Trans. Power Electron.*, vol. 24, no. 7, pp. 1826–1838, Jul. 2009.
[23] M. Kheraluwala, R. Gascoigne, D. Divan, and E. Baumann, "Performance characterization of a high-power dual active bridge dc-to-dc converter," *IEEE Trans. Ind. Appl.*, vol. 28, no. 6, pp. 1294–1301, Nov. 1992.

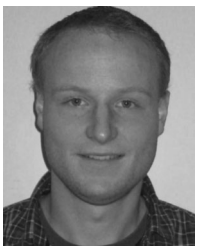

Nico H. Baars (S'13) received the B.Eng. degree in electrical engineering in 2010 from HAN University of Applied Sciences, Arnhem, The Netherlands. He received the M.Sc. degree in electrical engineering in 2013 from Eindhoven University of Technology, Eindhoven, The Netherlands, where he is currently working toward the Ph.D. degree at the Department of Electrical Engineering in the group Electromechanics and Power Electronics.

His research interests include electric drives and high-power converters.

Jordi Everts (S'09–M'13) received the M.Sc. degree (*magna cum laude*) from the Limburg Catholic University College, Limburg, Belgium, in 2007, and the Dr.Sc. degree from the University of Leuven, Leuven, Belgium, in 2014.

He is currently an Assistant Professor of power electronics at the EE-EPE Division of the Eindhoven University of Technology, Eindhoven, The Netherlands. In 2011 and 2012, he was a visiting Researcher at the Power Electronic Systems Laboratory, Swiss Federal Institute of Technology Zurich, Zurich, Switzerland. From 2009 to 2013, he held a Ph.D. fellowship from the Institute for the Promotion of Innovation through Science and Technology in Flanders (IWT-Vlaanderen). His research interests include the analysis, design, control, and optimization of high-frequency power converters. He has published several international papers and patents.

Henk Huisman (M'93) was born in Gouda, The Netherlands, in 1958. He received the M.Sc. and Ph.D. degrees from Delft University of Technology, Delft, The Netherlands, in 1984 and 1992, respectively.

He has been a Research Scientist in the Laboratory for Power Electronics, Delft University, Delft, and also in the Systems and Control Group. Later, he joined CCM, Nuenen, The Netherlands, where he was engaged on high-speed drives for flywheel applications. Since 2006, he has been a Staff Member at Philips Electronics, Eindhoven, The Netherlands, and since 2010, as a Part-Time Assistant Professor at Eindhoven University of Technology, Eindhoven. In both capacities, he has been involved on the analysis and design of high-precision power amplifiers. He has authored several papers on multiphase series-resonant power converters, flywheel applications, and various other topics. His current research interests include power electronics, application of chaos theory in system development, simulation, and control design.

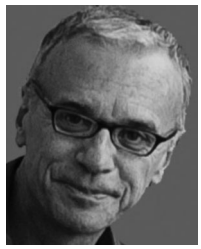

Jorge L. Duarte (M'99) received the M.Sc. degree in 1980 from the University of Rio de Janeiro, Rio de Janeiro, Brazil, and the Dr.-Ing. degree in 1985 from the Institut National Polytechnique de Lorrain-Nancy, Nancy, France, all in electrical engineering.

From 1988 to 1989, he was appointed as a Research Engineer at Philips Lighting Central Development Laboratory, Eindhoven, The Netherlands. In 1990, he joined the Electrical Engineering Department, TU Eindhoven, Eindhoven, as an Assistant Professor, where he teaches power electronics. Since 2000, he has also been engaged in independent consultant work on a regular basis for high-tech industries around Eindhoven. His current research interests include sampled-data modeling, nonlinear control, and real-time programming of power electronic systems.

Elena A. Lomonova (SM'02) was born in Moscow, Russia. She received the M.Sc. (*cum laude*) and Ph.D. (*cum laude*) degrees in electromechanical engineering from Moscow State Aviation Institute, Moscow, in 1982 and 1993, respectively.

Since 2008, she has been a Full Professor and the Head at Electromechanics and Power Electronics Group, Eindhoven University of Technology, Eindhoven, The Netherlands. She has worked on electromechanical actuator designs, power-train and energy conversion systems, and optimization and development of advanced mechatronic systems.